TEC CALIBRATION TO DETECT EQUATORIAL PLASMA BUBBLES WITH SINGLE FREQUENCY GNSS DATA

Ana L. Christovam*(1), Fabricio S. Prol (2), and Paulo O. Camargo(1)
(1) Department of Cartography, São Paulo State University (UNESP), Presidente Prudente, São Paulo 19060-900, Brazil
(2) Department of Navigation and Positioning, Finnish Geospatial Research Institute, National Land Survey of Finland, 02150 Espoo, Finland

Abstract

This study investigates the feasibility of employing a straightforward method for real-time Total Electron Content (TEC) determination based on single frequency GNSS data. TEC values derived from GNSS single frequency data was compared to dual frequency TEC estimative, revealing close agreement, with discrepancies of around ±2.5 TECU. The expected noisier nature of single frequency data is attributed to overall noise and multipath effects. However, despite the inherent code noise from the single frequency GNSS combination, the proposed method was efficient for mapping ionospheric plasma bubbles. The proposed calibration method emerges as an efficient tool for real-time mapping of ionospheric plasma bubbles, offering advantages over global-scale ionospheric models.

1. Introduction

Several studies have presented a close relationship between the presence of ionospheric plasma bubble and severe ionospheric scintillations at different radio signals observed at low latitudes [1-4]. Higher frequency radio signals present smaller changes in ionospheric refractive index compared to lower frequency signals [5-6]. As a result, lower frequency radio signals are more susceptible to stronger ionospheric scintillations. Considering the GPS signals, it is therefore expected that the GPS L2 signal will suffer greater ionospheric interference when compared to the GPS L1 signal under the influence of ionospheric scintillation. In this regard, using single frequency GNSS data in the L1 frequency can be considered a viable alternative for ionospheric imaging of plasmas bubbles.

Recently, [7-8] developed a regional ionospheric model capable of detecting ionospheric plasma bubbles in the Brazilian region using single frequency GNSS data. A main drawback of the proposed approach is that many GNSS stations are required to implement this method effectively. An alternative to estimate TEC with less requirements on the number of regional stations is performing TEC calibration procedures. Several studies have used TEC calibration methods [9-13]. In summary, the TEC calibration method involves determining the receiver and satellite hardware biases for each individual station. Besides requiring less computational effort, one of the benefits of the TEC calibration method is that it enables estimation for a single station without relying on a dense GNSS network. Aiming to investigate the feasibility of using GNSS single frequency data to detect plasma bubbles with no dependence on several GNSS stations, we developed in this work a TEC calibration method. The main goal is to reproduce the results obtained in [7] but using TEC solutions that are obtained individually for each GNSS station.

2. TEC Calibration

For TEC estimation with single frequency GNSS data, the combination between the observables $P1 - L1$ so-called Code-Minus-Carrier (CMC) is used. It eliminates all the terms independent on the frequencies, such as the tropospheric delay, clocks, and geometric distance. The TEC for each epoch is computed using the following equation:

$$TEC_{SF} = K \times ((P_1 - L_1\lambda_1) + BF_{SF}) \qquad (1).$$

where P_i and L_i are the GNSS pseudorange and carrier phase for frequency f_i, respectively, λ_i is the wavelength in meters; n_{obs} represents the number of observations in arc with continuous data. The K term converts meters of delay to the electrons/m^2 units, being $K = \left(f_{L1}{}^2/(2 \times 40.3)\right)$. B_{SF} represents the bias term and the residual errors. The bias term (B_{SF}) over one arc of data with no cycle slips is estimated using TEC^{inx} retrieved by Global Ionospheric Models (GIMs), as following:

$$B_{SF} = \frac{1}{n_{obs}} \sum_{j=1}^{n_{obs}} (L_1\lambda_1 - P_1) + \frac{TEC^{inx}}{K} \qquad (2).$$

By substituting equation (2) in (1), we then obtain the calibrated form of TEC.

3. Results

To perform a validation of the TEC calibration procedure, the STEC values obtained with single and dual frequency were compared. Three representative stations are chosen to cover different latitudinal regions of the ionosphere, belonging to RBMC (Brazilian Network for Continuous GNSS Monitoring). The selected stations are BELE (1.4° S, 48.5° W), CHPI (22.7° S, 45.0° W); and POAL (30.1° S, 51.1° W). BELE station is located near the geomagnetic equator, CHPI is located near the southern crest of the equatorial anomaly whereas POAL is closer to the mid-latitude region. The STEC data are computed for day 006 of 2014, when clear ionospheric plasma bubble occurred. In addition, it is considered a 30° cut-off elevation angle to avoid multipath errors.

Figure 1 shows a comparative example of STEC values obtained by the calibration procedure with single (left panel) and dual frequency (right panel) data for selected station. The values are expressed in TEC Units (TECU – 10^{16} el/m²). It can be noted that daily behavior between the results is similar. As expected, the STEC values obtained with single frequency are noisier than the dual frequency values. This is mainly justified due to the observable (pseudorange) used in the CMC model, which is nosier than the carrier phase combination.

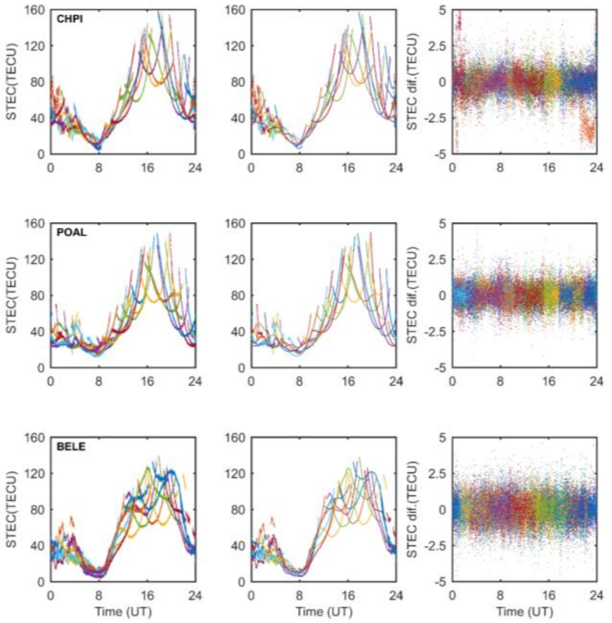

Figure 1. STEC values estimated for DOY 006 of 2014 at CHPI, POAL and BELE stations. The left panel shows the STEC values obtained with single frequency whereas the right panel presents with dual frequency. The different colors represent different GPS satellites.

BELE and POAL stations presented a similar behavior. The discrepancies vary between ±2.5 TECU where this difference corresponds to the noise level of pseudorange measurements. The largest discrepancies were obtained for CHPI, reaching up ± 5 TECU. CHPI is located in the region with the highest ionospheric variability. Due to seasonal variations, during the solstice months (summer), the electron density ambient and the plasma density gradients are more intense to produce ionospheric irregularities, with much higher variabilities in the latitude of CHPI. Three parameters were used to evaluate the discrepancies between single and dual frequency data: mean, standard deviation (STD), and the root mean- square (RMS) of the difference. A summary of the statistical information of the is listed in Table 1.

Table 1. Mean, standard deviation, and root mean square of the difference between single and dual frequency for DOY003, 2014. The statics values are presented in TECU.

Stations	Mean (TECU)	STD (TECU)	RMS (TECU)
POAL	0.0001	0.5850	0.5850
CHPI	0.0782	1.5431	1.5452
BELE	0.0003	0.7393	0.7393

In general, the mean discrepancy tends to zero, which means that there is no systematic difference between the methods for representing the daily behavior of STEC. The higher discrepancies were obtained for CHPI followed by BELE and POAL stations. In terms of STD and RMSD, the POAL and BELE stations presented similar statistical values, whereas the CHPI showed approximately twice as many values. The STEC values obtained with single frequency were acceptable, with the discrepancies corresponding the random noise level.

4. Ionospheric Maps

In this section, we present maps obtained with single frequency data and compare them with the ones obtained based on dual frequency data. GNSS data from 189 stations from IGS, RBMC, RAMSAC (Red Argentina de Monitoreo Satelital Continuo), CIGALA/CALIBRA (Countering GNSS high Accuracy applications Limitations due to Ionospheric disturbances in Brazil), and LISN (Low latitude Ionospheric Sensor Network) networks are used. The location of GNSS stations used for the regional maps are shown in Figure 2 (left panel).

Figure 2 (right panel) provide an idea of the spatial distribution of the IPPs available for DOY 032 of 2014 at 1.8 h TU. The IPPs are obtained assuming an ionospheric peak height at 450 km altitude. It can be noted a low number of IPPs in the Amazon Forest, impairing the spatial resolution in this area. In addition, the ionospheric plasma bubble can be seen aligned with the geomagnetic equator, located at 50° W and 20º S, which is characterized by the depletion surrounded by higher VTEC values.

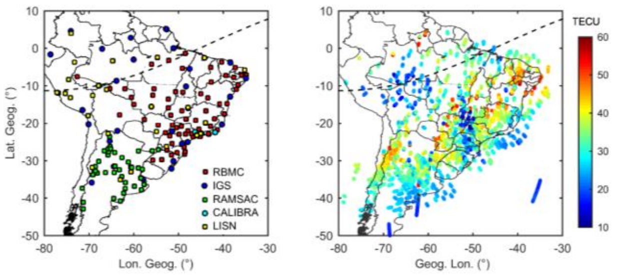

Figure 2. Location of GNSS stations used in ionospheric maps (left panel). The dashed line represents the Magnetic Equator. The right panel shows the IPPs spatial distribution for DOY 032 of 2014, at 1.8 h TU.

To evaluate the TEC maps obtained with single frequency data, the maps obtained with single and dual frequency data were compared. Figure 3 shows a sequence of VTEC maps for DOY 032 of 2014 with single (top panel) and dual frequency (middle panel) with a temporal evolution of 6 min, as well as the difference (bottom panel). It can be noted that the ionospheric maps are similar. The bottom panel shows that the discrepancies were around ± 2 TECU, however, the largest differences are centered on zero. The largest discrepancies are in the EIA region, due to the higher ionospheric variability. In this region, the high level of ionospheric irregularities is responsible for the generation of ionospheric scintillations in the GNSS signals, which produces GNSS loss of lock and reinitializations of the TEC calculation. VTEC mapping for single and dual frequency provide large-scale coverage of the plasma bubbles. In both maps, it can be seen the formation and evolution progress of the two plasma bubbles characterized by depletion in VTEC values represented by elongated tubes. Although the TEC data obtained with single frequency is noisier than the dual frequency data, it is possible to successfully observe the ionospheric plasma bubbles**.**

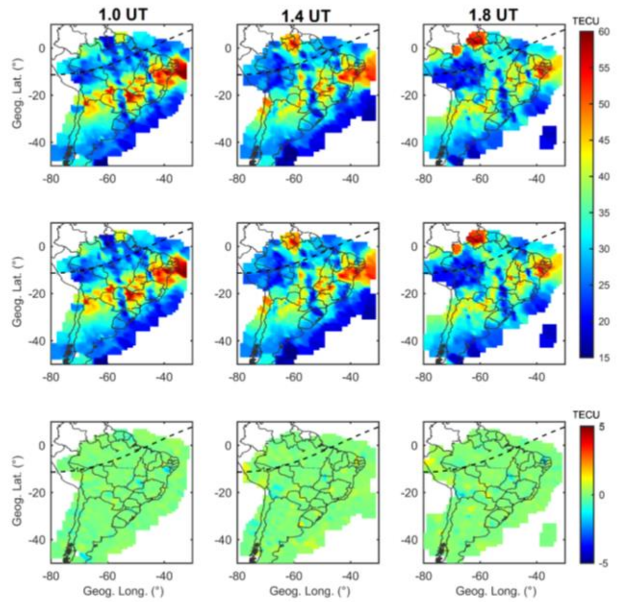

Figure 3. Comparison of VTEC maps, for DOY 032 of 2014 between 1.0 UT to 1.8 UT. The top and central panel represents the TEC maps obtained with TEC dual and single frequency, respectively. The bottom panel shows the difference between single and dual frequency.

5. Conclusion

This study explores the viability of using a straightforward method for determining TEC values based on single frequency GNSS data for prospective real-time applications. In order to accomplish this, a TEC calibration method is presented. For the validation, TEC obtained with single and dual frequency were compared. The single and dual frequency data showed quite similar values. The discrepancies were around ± 2.5 TECU. As expected, TEC values obtained with single frequency were noisier to those obtained with dual frequency. The main difference corresponds to the overall noise level and multipath coming from the GNSS combination.

Analyzing the VTEC maps, it was confirmed the possibility to detect the ionospheric plasma bubbles based on single frequency GNSS data. The ionospheric maps obtained from single frequency data presented a good imaging of the plasma bubbles. It is important to mention that the code noise issues from the CMC combination was not able to impair the plasma bubble imaging.

6. Acknowledgements

We acknowledge the Technology for GNSS in Support of Air Navigation (INCT GNSS-NavAer), funded by CNPq (465648/2014-2), FAPESP (2017/50115-0) and CAPES (88887.137186/2017-00). This study was financed in part by the Coordenação de Aperfeiçoamento de Pessoal de Nível Superior—Brasil (CAPES)—Finance Code 001 and CNPq (117659/2023-4).

References

[1] L. Spogli, C. Cesaroni, D. Di Mauro, M. Pezzopane, L. Alfonsi, E. Musicò, N. Floury, "Formation of ionospheric irregularities over Southeast Asia during the 2015 St. Patrick's Day storm," Journal of Geophysical Research: Space Physics, vol. 121, no. 12, pp. 12,211-12,233, 2016, doi: 10.1002/2016ja023222.

[2] C. Xiong, C. Stolle, H. Lühr, "The Swarm satellite loss of GPS signal and its relation to ionospheric plasma irregularities," Space Weather, vol. 14, no. 8, pp. 563-577, 2016, doi: 10.1002/2016SW001439.

[3] A. O. Moraes, B. C. Vani, E. Costa, M. A. Abdu, E. R. de Paula, J. Sousasantos, M. H. Shimabukuro, "GPS availability and positioning issues when the signal paths are aligned with ionospheric plasma bubbles," GPS Solutions, vol. 22, pp. 1-12, 2018, doi: 10.1007/s10291-018-0760-8.

[4] A. L. C. Souza, G. O. Jerez, P. D. O. Camargo, D. B. M. Alves, "Assessment of GPS positioning performance using different signals in the context of ionospheric scintillation: a month-long case study on São José dos Campos, Brazil," Boletim de Ciências Geodésicas, vol. 28, 2022, doi: 10.1590/s1982-2170202200040001.

[5] K. C. Yeh, C. H. Liu, "Radio wave scintillations in the ionosphere," Proceedings of the IEEE, vol. 70, no. 4,pp.324-360,1982, doi: 10.1109/PROC.1982.12313.

[6] A. Bhattacharyya, "Equatorial plasma bubbles: a review," Atmosphere, vol. 13, no. 10, p. 1637, 2022, doi: 10.3390/atmos13101637

[7] A. L. Christovam, F. S. Prol, M. Hernández-Pajares, P. O. Camargo, "Plasma bubble imaging by single-frequency GNSS measurements," GPS Solutions, vol. 27, no. 3, p. 124, 2023, doi: 10.1007/s10291-023-01463-z

[8] A. L. Christovam, F. S. Prol, M. Hernández-Pajares, P. O. Camargo, "PPP at low latitudes with ionospheric model exclusively based on single frequency GNSS measurements," Space Weather, vol. 21, no. 8, 2023, doi.org/10.1029/2023SW003513

[9] L. Ciraolo, F. Azpilicueta, C. Brunini, A. Meza, S. M. Radicella, "Calibration errors on experimental slant total electron content (TEC) determined with GPS," Journal of Geodesy, vol. 81, pp. 111–120, 2007, doi: 10.1007/s00190-006-0093-1.

[10] F. E. Z. A. Arikan, H. Nayir, U. M. U. T. Sezen, O. Arikan, "Estimation of single station inter frequency receiver bias using GPS-TEC," Radio Science, vol. 43, no. 04, pp. 1-13, 2008, doi: 10.1029/2007rs003785.

[11] O. Montenbruck, A. Hauschild, P. Steigenberger, "Differential code bias estimation using multi - GNSS observations and global ionosphere maps," Navigation: Journal of the Institute of Navigation, vol. 61, no. 3, pp. 191-201, 2014, doi: 10.1002/navi.64.

[12] F. S. Prol, P. O. Camargo, "Estimativa da tendência diferencial do código nos receptores GNSS," Boletim de Ciências Geodésicas, vol. 20, pp. 735-749, 2014, doi: 10.1590/S1982-21702014000400042.

[13] F. S. Prol, M. Hernández-Pajares, M. T. A. H. Muella, P. O. Camargo, "Tomographic imaging of ionospheric plasma bubbles based on GNSS and radio occultation measurements," Remote Sensing, vol. 10, no. 10, p. 1529, 2018, doi: 10.3390/rs10101529.